

# Contact-induced Damage in Ceramic Coatings on Compliant Substrates: Fracture Mechanics and Design

Young-Woo Rhee,<sup>†</sup> Hae-Won Kim,<sup>‡</sup> Yan Deng,<sup>§</sup> and Brian R. Lawn<sup>\*\*</sup>

Materials Science and Engineering Laboratory, National Institute of Standards and Technology, Gaithersburg, Maryland 20899

Simple explicit relations are presented for the onset of competing fracture modes in ceramic coatings on compliant substrates from Hertzian-like contacts. Special attention is given to a deleterious mode of radial cracking that initiates at the lower coating surface beneath the contact, in addition to traditional cone cracking and quasiplasticity in the near-contact area. The critical load relations are expressed in terms of well-documented material parameters (elastic modulus, toughness, hardness, and strength) and geometrical parameters (coating thickness and sphere radius). Data from selected glass,  $\text{Al}_2\text{O}_3$ , and  $\text{ZrO}_2$  coating materials on polycarbonate substrates are used to demonstrate the validity of the relations. The formulation provides a basis for designing ceramic coatings with optimum damage resistance.

## I. Introduction

CERAMIC coatings on compliant substrates are used in many engineering applications (cutting tools, thermal barrier coatings, electronic multilayers, and laminated windows), biological structures (teeth and dental crowns, and shells), and traditional pottery (ceramic glazes). A hard coating provides enhanced load-bearing capacity, wear resistance, thermal and corrosion protection, electrical insulation, and aesthetics; a compliant substrate provides stress redistribution and damage tolerance. Yet despite the manifest importance of such applications, design strategies for optimizing coating parameters remain largely based on empirical methodologies, such as finite element analysis. There is a need for more analytical approaches, in which the critical conditions may be expressed explicitly in terms of conventional material parameters (elastic modulus, hardness, toughness, and strength) and geometrical variables (coating thickness and indenter radius).

This need is especially pressing in the case of contact loading, where severe damage may be incurred at relatively low applied loads.<sup>1,2</sup> In natural or restorative tooth structures, for instance, repeat biting forces as low as 100 N at contacts between opposing cusps of characteristic radii 2–4 mm can cause premature *in vivo* failures.<sup>3–5</sup> The stress field in the supported coating is Hertzian-like in the near-contact region and flexure-like in the far-contact region, with resultant competing modes of fracture and damage in the coating. These modes include traditional cone cracks and

subsurface quasiplasticity in the Hertzian near-contact region<sup>1,6–9</sup> and a form of radial crack in the flexural field at the lower coating surface beneath the contact, unique to layer structures.<sup>5,10–18</sup> Delamination is not observed to be a principal mode of contact damage in such structures, even weak (epoxy adhesive) interfaces, at least in single-cycle loading.<sup>16,17,19</sup> The radial cracks are particularly deleterious because they can initiate at relatively low loads (especially in thinner coatings) and can spread over long distances. They also tend to remain subsurface, and are therefore not always observable from routine surface inspection, even though failure may be imminent. Whereas explicit relations for critical loads have been well documented for the cone cracking and quasiplasticity modes, analogous relations for lower-surface radial cracking have only recently been considered.<sup>16,17</sup>

Here we develop a design strategy for optimizing resistance to Hertzian-type damage in ceramic coating systems. Simple analytical relations for the critical loads for the onset of each damage mode are first derived in terms of conventional material parameters (elastic modulus, hardness, toughness, and strength) and geometrical variables (coating thickness, and indenter radius). Contact testing is then performed on glass,  $\text{Al}_2\text{O}_3$  and  $\text{ZrO}_2$  outer layers bonded with epoxy adhesive to polycarbonate underlayers in order to validate these relations. The ceramics are chosen for their broad range of properties; the polycarbonate and adhesive are conveniently transparent, enabling *in situ* subsurface observation of radial crack initiation.<sup>16,17</sup> With the validity of the relations thus established, design diagrams are constructed to determine the domains of “safe operation” for any given material system.

## II. Critical Load Relations

The system under consideration is shown schematically in Fig. 1. The specimen consists of an infinitely wide flat ceramic coating of thickness  $d$  bonded with adhesive to a compliant polycarbonate substrate (S), with relative elastic modulus  $E/E_s$ . The properties of the adhesive are considered to match those of the substrate, so that the system is essentially a bilayer.<sup>16</sup> A spherical indenter of radius  $r$  is impressed onto the coating surface at load  $P$ , with associated contact radius  $a$ . Three types of damage may be initiated within the coating:<sup>2</sup> *cone cracks* (C) at the upper surface immediately outside the contact; *quasiplasticity* in a yield zone (Y) immediately beneath the contact; and *radial cracks* (R) at the lower coating surface, directly below the contact.

### (I) Radial Cracks

Radial cracks owe their origin to flexure induced by the indentation of the coating on a relatively compliant substrate.<sup>11,12,16,17</sup> The lower surface directly below the contact is stressed in biaxial tension. In the domain of small contacts ( $a \ll d$ ) the indentation may be approximated by a center point force. Then the maximum tensile stress has the simple dependence  $\sigma \propto P/d^2$  characteristic of plates in axisymmetric bending.<sup>20</sup> Due allowance for the presence of a soft base introduces an additional, modulus mismatch factor  $\log(CE/E_s)$  into  $\sigma$ , to accommodate the compliance of the support.<sup>20,21</sup>

G.M. Pharr—contributing editor

Manuscript No. 188440. Received June 22, 2000; approved November 20, 2000. Supported by grants from the Korean Science and Engineering Foundation (author YWR) and the U.S. National Institute of Dental Research.

<sup>\*\*</sup>Fellow, American Ceramic Society.

<sup>†</sup>Department of Materials Science and Engineering, Korea Advanced Institute of Science and Technology, Yusong, Taejeon 305-701, Korea.

<sup>‡</sup>School of Materials Science and Engineering, Seoul National University, Seoul 151-742, Korea.

<sup>§</sup>Department of Materials and Nuclear Engineering, University of Maryland, College Park, MD 20742.

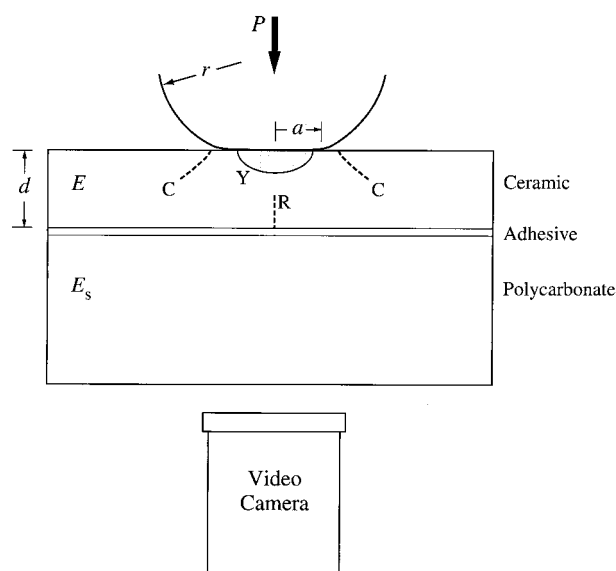


**Fig. 1.** Schematic showing damage modes in ceramic/polycarbonate bilayer from indentation with sphere: radial cracking (R), cone cracking (C), and quasiplasticity (Y).

Radial cracking is assumed to initiate spontaneously from a starting flaw in the lower coating surface at a critical load  $P_R$  when the maximum tensile stress  $\sigma$  equals the bulk flexure strength  $\sigma_F$  of the coating. For infinitely wide specimens we obtain, in the limit of small contacts and coating surface displacements,<sup>20</sup>

$$P_R = \frac{B\sigma_F d^2}{\log(CE/E_s)} \quad (1)$$

with  $B$  and  $C$  dimensionless coefficients. Values  $B = 2.04$  and  $C = 0.94$  have been “calibrated” in a preceding study from fits to data on model glass/substrate bilayer systems.<sup>22</sup> In the limit  $E_s \rightarrow E$ , we obtain  $P_R \rightarrow \infty$  for  $C \approx 1$ , which is consistent with the observed absence of flexure-induced radial cracking in monoliths. A feature of Eq. (1) is the strong, quadratic dependence of  $P_R$  on  $d$ , indicating that thin coatings are particularly vulnerable. The controlling material parameters are  $\sigma_F$  and  $E/E_s$ , although the dependence on the latter is comparatively weak. The appearance of  $\sigma_F$  means that  $P_R$  is sensitive to the surface flaw state.

$P_R$  in Eq. (1) is independent of  $r$ , at least in the limit  $a \ll d$ . Correction factors for the more general case of nonzero  $a/d$  exist,<sup>20</sup> but are omitted here for the sake of simplicity.

## (2) Cone Cracks and Quasiplasticity

As indicated, cone cracks and quasiplasticity are induced in the contact near field, the first mode by the tensile component and the second by the shear component. As a first approximation, we may simplify matters by neglecting any modifying effects on the surface stress state from the underlying substrate.

In a preceding article, it was shown that the critical loads  $P_C$  and  $P_Y$  for cone cracking and yield in monoliths may be expressed as functions of basic material parameters,<sup>9</sup> from well-established

Hertzian contact theory. Now the indenter modulus  $E_i$  becomes important. Let us define an “effective modulus”  $E' = 1/(1/E + 1/E_i)$ . For cone cracks, the critical load is given by Auerbach’s Law<sup>2,23,24</sup>

$$P_C = A \left( \frac{T^2}{E'} \right) r \quad (2)$$

with  $A = A(\nu)$  a dimensionless coefficient ( $\nu$  is Poisson’s ratio) and  $T$  is the toughness ( $K_{IC}$ ). For quasiplasticity, the critical load is

$$P_Y = DH \left( \frac{H}{E'} \right)^2 r^2 \quad (3)$$

with  $D$  another dimensionless coefficient and  $H$  the indentation hardness (load/projected area, Vickers indentation). Calibration values  $A = 8.6 \times 10^3$  and  $D = 0.85$  have been determined from fits to data on a range of ceramics.<sup>9</sup> Thus, controlling material parameters in these modes are  $E$ ,  $T$ , and  $H$ . Because these parameters are insensitive to flaw state (notwithstanding the fact that surface flaws are necessary to initiate cone cracks<sup>23,25</sup>), so are  $P_C$  and  $P_Y$ .  $P_C$  and  $P_Y$  are also insensitive to  $d$ , reflecting a near-field approximation implicit in the derivations of Eqs. (2) and (3) for first damage inception.

It is implicit here that the toughness is independent of crack size; the existence of an  $R$ -curve tends to diminish  $H$  as it enhances  $T$ , effecting a type of (microstructurally controlled) brittle–plastic transition.<sup>26,27</sup> The different dependencies of  $P_C$  and  $P_Y$  on  $r$  in Eqs. (2) and (3) indicate another type of brittle–plastic transition, as the manifestation of an indentation size effect.<sup>9</sup>

For specimens with surface curvature  $r_{\text{surf}}$ ,  $r$  is replaced by an “effective radius”  $r' = 1/(1/r + 1/r_{\text{surf}})$ .<sup>9,28</sup>

## III. Experiment<sup>¶</sup>

### (1) Materials and Fabrication

Three well-behaved ceramics covering a broad range of material properties were chosen as coating materials: (i) *soda-lime glass*, the quintessential brittle material, providing a convenient reference baseline; (ii)  $\text{Al}_2\text{O}_3$  (AD999, Coors Ceramics, Golden, CO), a relatively pure, fine-grain ceramic with intermediate properties; and (iii)  $\text{ZrO}_2$  (Y-TZP, Norton–St. Gobain, Raleigh, NC), another fine-grain,  $\text{Y}_2\text{O}_3$ -stabilized tetragonal  $\text{ZrO}_2$  polycrystal, with exceptionally high strength but some tendency to plasticity.<sup>9</sup> A polycarbonate plastic (AIN Plastics, Norfolk, VA) was selected for the substrate, because of its transparency and relatively small time dependence in the indentation load–displacement response.<sup>16</sup> Material parameters for these materials are listed in Table I.

Each ceramic material was prepared in the form of slabs with a minimum lateral surface dimension 15 mm. Surfaces were ground and polished (1  $\mu\text{m}$  diamond) to thicknesses in the range 0.1–6 mm. Because the polycrystalline ceramics contained a sufficient density of intrinsic microstructural flaws for subsequent crack initiation, their surfaces were tested as-polished, after gold

<sup>¶</sup>Information on product names and suppliers in this article is not to imply endorsement by NIST.

**Table I. Mechanical Properties for Constituent Layer and Indenter Materials<sup>†</sup>**

Material	Young’s modulus, $E$ (GPa)	Hardness, <sup>‡</sup> $H$ (GPa)	Toughness, $T$ ( $\text{MPa}\cdot\text{m}^{1/2}$ )	Strength, <sup>§</sup> $\sigma_F$ (MPa)	Reference
Soda-lime glass	70	5.2	0.67	$110 \pm 9$	9, 16
Alumina (AD999)	390	17.5	3.1	$460 \pm 63$	9, 29
Zirconia (Y-TZP)	205	12.0	5.4	$1450 \pm 250$	9, 30
Polycarbonate	2.3	0.14			9, 16
Tungsten carbide	614	16.0			9, 31

<sup>†</sup>Uncertainties in  $E$  estimated at  $< 5\%$ , in  $H < 10\%$  and  $T < 20\%$ . Errors in  $\sigma_F$  are experimental standard deviations. <sup>‡</sup>Indentation hardness,  $H = 2P/d^2 = 1.078H_V$ ,  $d$  = indent diagonal. <sup>§</sup>As-polished surfaces, except glass surfaces abraded (600 SiC grit).

coating the lower surfaces to enhance reflectivity for subsequent subsurface viewing. The soda-lime glass surfaces were given post-polish abrasion treatments with a slurry of 600 SiC grit to provide uniform, extrinsic flaw densities.<sup>16</sup> The polycarbonate bases were used in their as-received, smooth-surface states, with a fixed thickness of 12.7 mm.

The glass and ceramic coating layers were bonded to the polycarbonate substrates using an epoxy adhesive (Harcos Chemicals, Bellesville, NJ) under light pressure for 24 h. The resultant adhesive layer was 10–20  $\mu\text{m}$  thick, and transparent. Because the bond was formed at ambient temperatures, thermal expansion mismatch stresses are not an issue. The elastic properties of the adhesive are similar to those of the polycarbonate base,<sup>16,32</sup> so that the finished laminate may be regarded as an ideal ceramic/substrate bilayer.

## (2) Contact Tests

Hertzian tests were conducted on the layer structures using WC spheres mounted into the crosshead of an Instron universal testing machine (Model 1122, Instron, Canton, MA). Most tests were done with spheres with a radius of  $r = 3.96$  mm; a select few were conducted at  $r = 1.0$ – $12.7$  mm. Loads were applied at a fixed crosshead speed of 0.15 mm/min, in air.

Radial crack initiation was monitored *in situ* from below the contact through the adhesive/polycarbonate sublayer, using an optical zoom system (Optem, Santa Clara, CA) mounted into a video camcorder (Model XL1, Canon, Lake Success, NY). Acoustic signals from a piezoelectric transducer (LOCAN 320, Physical Acoustics Corp., Princeton, NJ) attached to the upper specimen surface with rubber cement provided complementary information on radial crack pop-in. Means and standard deviations for  $P_R$  were thereby determined from a minimum of five indentations on each specimen. Values of  $P_C$  for cone cracking in glass could also be measured in this way.<sup>16</sup>

An alternative procedure was necessary to determine the onset of cone cracking and quasiplasticity in the opaque ceramic coatings,<sup>9</sup> since these modes did not emit strong acoustic signals. Rows of indentations were made on each coating surface at incrementally increasing peak loads, and the surfaces examined *a posteriori* generally within an hour of indentation and gold coating using Nomarski illumination. (The Y-TZP specimens were examined within five minutes of indentation, in the uncoated state, to compensate for a marked time-dependent recovery of the residual impressions in this material, disappearing altogether within a few hours at loads just above threshold.<sup>9</sup>) Means and uncertainty bounds for  $P_C$  were determined from the load ranges at which surface ring cracks first appeared as incipient shallow arcs (lower limit) and were fully formed (upper limit). Values for  $P_Y$  were similarly determined as the load ranges over which the residual surface impressions were completely undetectable and were clearly visible.

## IV. Results and Analysis

### (1) Radial Crack Morphology

Figures 2–4 show micrographs of radial cracking in glass,  $\text{Al}_2\text{O}_3$  and  $\text{ZrO}_2$  coating specimens, taken from video recording sequences. Each sequence covers one complete loading–unloading cycle. The examples are for relatively thin coatings, near the lower end of the range covered, so as to encompass the entire crack patterns within a working field of view. In the case of glass coatings, surface abrasions are visible. The first micrograph in each case shows the lower surface of the coating at or around first radial crack initiation. The load corresponding to this near-initiation configuration is relatively small for the glass, high for the  $\text{ZrO}_2$ . Initiation itself is abrupt, with single opposing crack arms popping outward from the contact center. At increasing load the cracks multiply and extend stably, ultimately forming a “starburst” pattern. On unloading, the cracks appear to retract and close up, becoming near-invisible at full indenter withdrawal, especially in

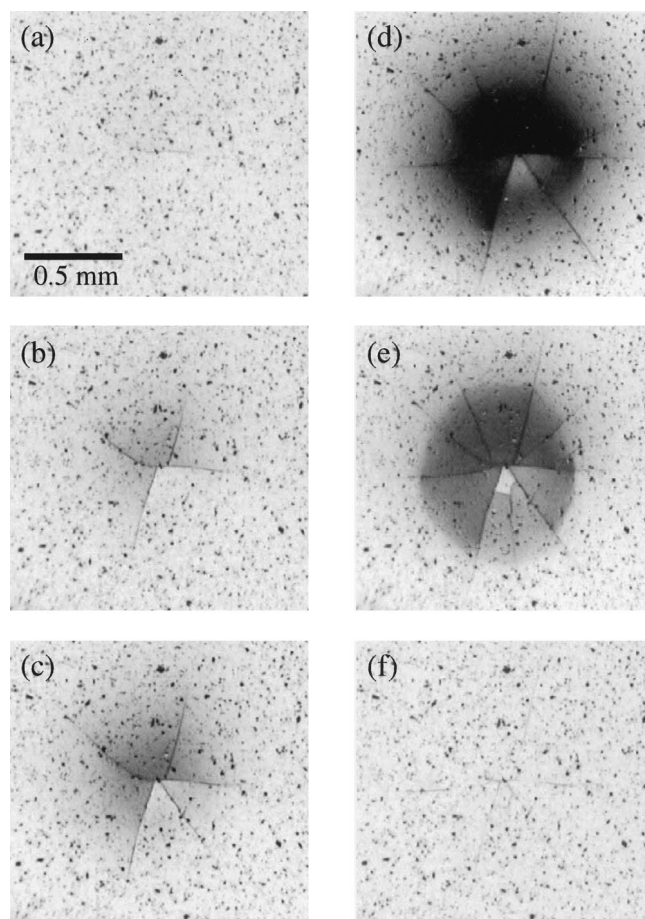


**Fig. 2.** Radial crack sequence in soda-lime glass coating,  $d = 180$   $\mu\text{m}$ , on polycarbonate substrate, thickness 12.7 mm, from indentation with WC sphere of  $r = 3.96$  mm. Loading half cycle, (a)  $P = 8.3$  N, (b)  $P = 13.4$  N, (c)  $P = 17.2$  N, (d)  $P = 37.6$  N; unloading half-cycle, (e)  $P = 25.2$  N, (f)  $P = 0$  N. Abrasion flaws on lower coating surface are visible.

the glass and  $\text{Al}_2\text{O}_3$ . However, the cracks do not heal; reloading reopens the original cracks.

In thicker specimens, the abruptness of the radial initiation event was much more pronounced, with multiple initiations more prevalent at higher critical loads. In extreme cases, at thicknesses  $d > 1$  mm or so, the cracks popped in to the specimen edges, sometimes causing spontaneous failure. Up to failure, the radial cracks remained subsurface during their extension.<sup>16</sup> All radial cracks were accompanied by acoustic emissions at pop-in, from barely detectable signals in the thinner materials to audible rings in the thicker ones. Similarly, load drops ranged from undetectable to  $>50\%$  over the same coating thickness range.

Cone cracks and quasiplasticity were more difficult to observe, because the surfaces could only be examined after the fact (in the  $\text{Al}_2\text{O}_3$  and  $\text{ZrO}_2$  at least).<sup>9</sup> The initiation events in these modes were not always abrupt or well-defined and were not generally accompanied by detectable acoustic signals or load drops.

### (2) Critical Loads

Critical load data for each of the polycarbonate-supported glass,  $\text{Al}_2\text{O}_3$ , and  $\text{ZrO}_2$  coating systems are shown in Figs. 5–7 as a function of  $d$ , at a fixed sphere radius of  $r = 3.96$  mm. Filled symbols are  $P_R$  data for radial cracking; the inclined solid lines are the corresponding *a priori* predictions from Eq. (1) using the material parameters in Table I. Unfilled symbols are  $P_C$  or  $P_Y$  data for cone cracking or yield, whichever of these two loads is the lower; the horizontal lines are the corresponding predictions from Eqs. (2) and (3). In the case of glass, the  $P_R$  data are obtained from specimens with lower surfaces abraded, and  $P_C$  from specimens with upper surfaces abraded. Thus, in thinner coatings (below  $d \approx$

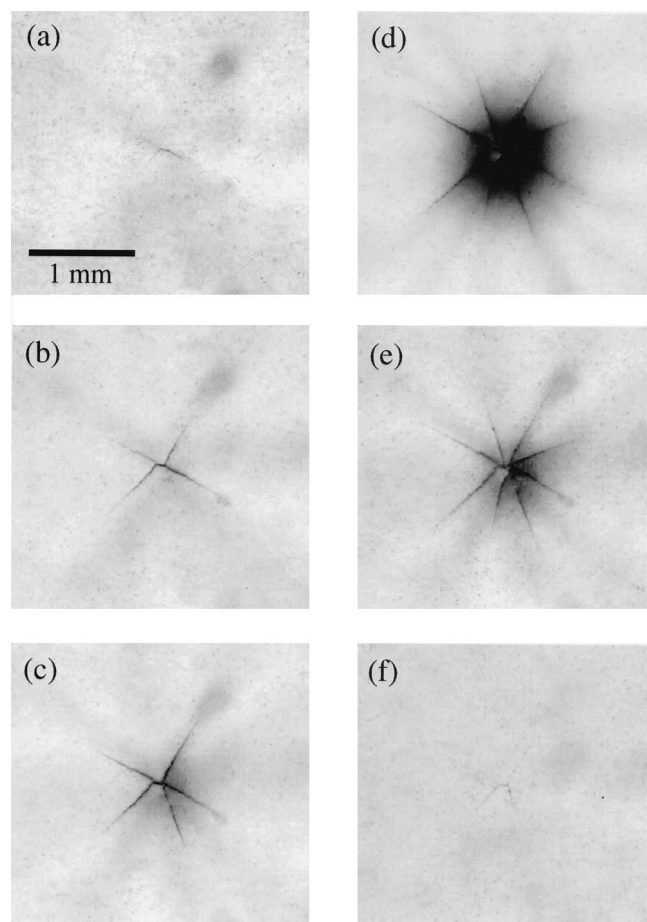


**Fig. 3.** Radial crack sequence in  $\text{Al}_2\text{O}_3$  (AD999) coating,  $d = 155 \mu\text{m}$ , on polycarbonate substrate, thickness 12.7 mm, from indentation with WC sphere of  $r = 3.96 \text{ mm}$ . Loading half cycle, (a)  $P = 15.1 \text{ N}$ , (b)  $P = 24.0 \text{ N}$ , (c)  $P = 35.1 \text{ N}$ , (d)  $P = 56.6 \text{ N}$ ; unloading half-cycle, (e)  $P = 33.3 \text{ N}$ , (f)  $P = 0 \text{ N}$ . Lower surface as-polished.

0.5–2.0 mm), radial cracks prevail. Of special note is the high sensitivity of  $P_R$  to  $d$  in this region, covering  $\sim 3$  orders of magnitude in Figs. 5–7. On this scale, deviations of a factor of 2 or more between data and predictions are not so consequential. In thicker coatings (above  $d \approx 0.5\text{--}2.0 \text{ mm}$ ), more conventional modes prevail, e.g. cone cracks in glass, quasiplasticity in  $\text{ZrO}_2$ , and both (indistinguishable) in  $\text{Al}_2\text{O}_3$ . In this region, the critical loads  $P_C$  or  $P_Y$  are relatively insensitive to  $d$ , as assumed in Section II.

Figure 8 shows critical loads for glass coatings as a function of  $r$ , at a fixed thickness of  $d = 1 \text{ mm}$ . Again, filled symbols are  $P_R$  data for radial cracking at abraded lower surfaces; the horizontal solid line is the corresponding prediction from Eq. (1).  $P_R$  is insensitive to  $r$ , again consistent with the assumption in Section II. Also plotted for comparison, are loads  $P_C$  (unfilled symbols), for abraded *monolithic* glass, along with the dashed line prediction from Eq. (2). Cone cracks could not be observed below loads of  $10^3 \text{ N}$  in the polycarbonate-supported glass coatings; instead, outer ring cracks formed well outside the contacts,<sup>16</sup> indicating a significant influence of the substrate on  $P_C$  in this case.

## V. Discussion

We have investigated conditions for the introduction of damage in ceramic coatings on compliant substrates subjected to concentrated loads. Specifically, we have identified principal damage modes in three coating materials on polycarbonate bases: glass, fine-grain  $\text{Al}_2\text{O}_3$ , and Y-TZP. These modes include conventional cone cracking and quasiplasticity at the top coating surface, in the

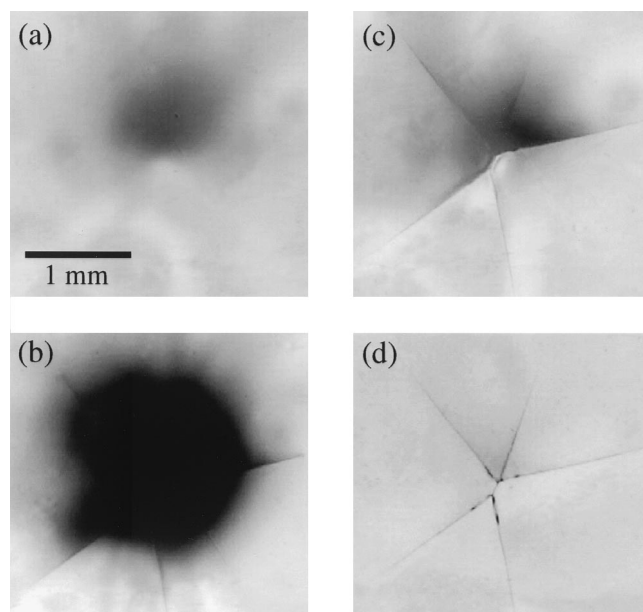


**Fig. 4.** Radial crack sequence in  $\text{ZrO}_2$  (Y-TZP) coating,  $d = 250 \mu\text{m}$ , on polycarbonate substrate, thickness 12.7 mm, from indentation with WC sphere of  $r = 3.96 \text{ mm}$ . Loading half cycle, (a)  $P = 119.5 \text{ N}$ , (b)  $P = 171.6 \text{ N}$ ; unloading half-cycle, (c)  $P = 69.5 \text{ N}$ , (d)  $P = 0 \text{ N}$ . Lower surface as-polished.

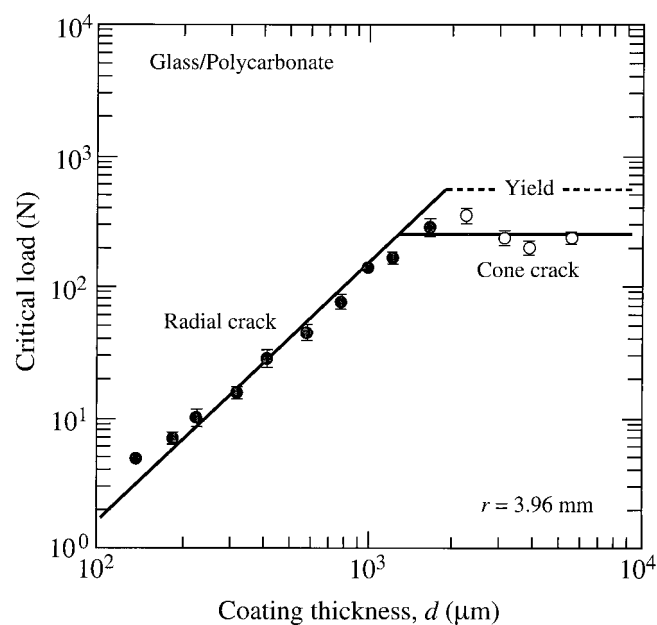


**Fig. 5.** Critical load as function of coating thickness  $d$  for soda-lime-glass/polycarbonate bilayers indented with WC spheres of  $r = 3.96 \text{ mm}$ . Filled symbols are  $P_R$  data, unfilled symbols are  $P_C$  data (quasiplastic mode not observed). Solid lines are theoretical predictions for radial and cone cracking and quasiplasticity (yield). Glass surfaces abraded with 600 grit SiC.

near-contact region (as seen in monoliths), and radial cracking at the lower coating surface, where flexural stresses are manifest. Delamination was not observed to be a common mode of cracking in our systems, despite the relatively weak (epoxy) adhesive used to join the coatings to the substrates. The radial cracks are especially deleterious because they can extend over comparatively large distances, in excess of several millimeters in our coatings, leading to failure at comparatively low loads. Consequently, the radial crack mode warrants singular attention in brittle coating structures (notwithstanding the fact that the other modes can also

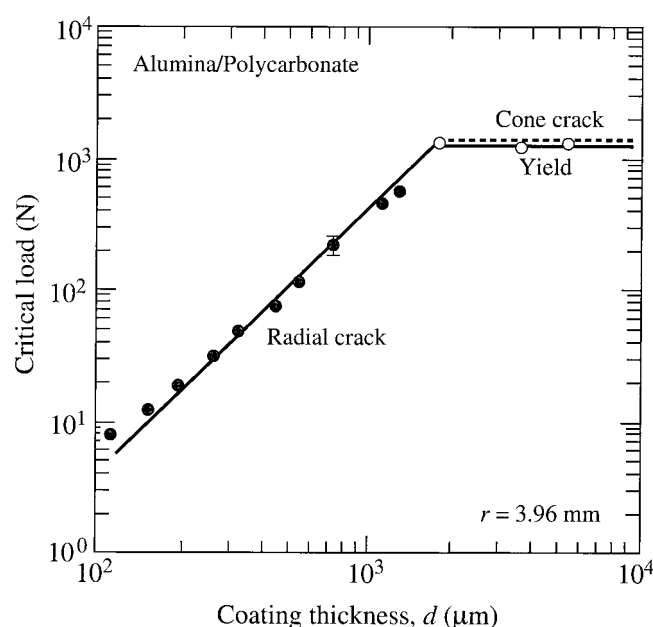


**Fig. 6.** Critical load as function of coating thickness  $d$  for  $\text{Al}_2\text{O}_3$ /polycarbonate bilayers indented with WC spheres of  $r = 3.96$  mm. Filled symbols are  $P_R$  data, unfilled symbols are  $P_C$  and  $P_Y$  data (indistinguishable). Solid lines are theoretical predictions for radial and cone cracking and quasiplasticity (yield).

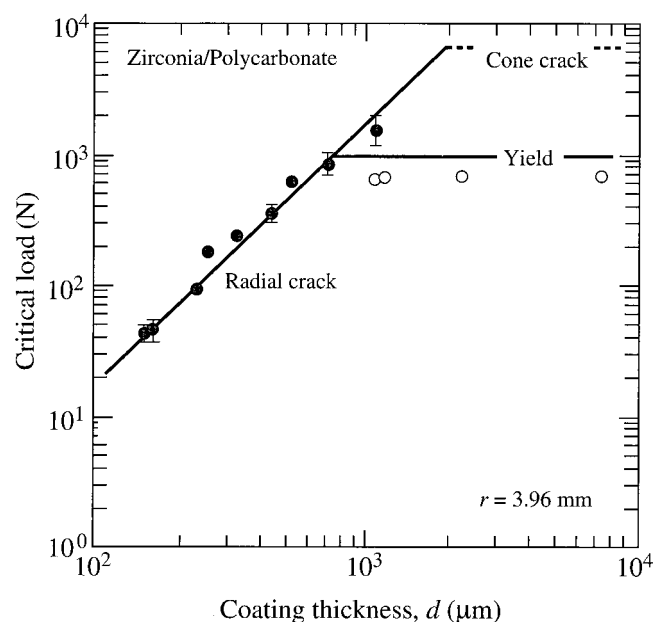


**Fig. 7.** Critical load as function of coating thickness  $d$  for  $\text{ZrO}_2$ /polycarbonate bilayers indented with WC spheres of  $r = 3.96$  mm. Filled symbols are  $P_R$  data, unfilled symbols are  $P_Y$  data (cone crack mode not observed). Solid lines are theoretical predictions for radial and cone cracking and quasiplasticity (yield).

lead to severe damage in brittle structures, especially in cyclic loading and under severe environmental conditions.<sup>33,34</sup>) The particular danger of the radial cracks is that they tend to remain subsurface up to the point of failure, making them difficult to detect from ordinary surface inspections or even from subsurface inspections through a transparent base (Figs. 2–4), because of crack closure on removal of the contact forces.

The determining geometrical variables in the critical loads to initiate each fracture mode are  $d$  and  $r$ . As seen in Figs. 5–7, radial cracking is the principal mode in thinner coatings ( $d < 0.5$ –2 mm).

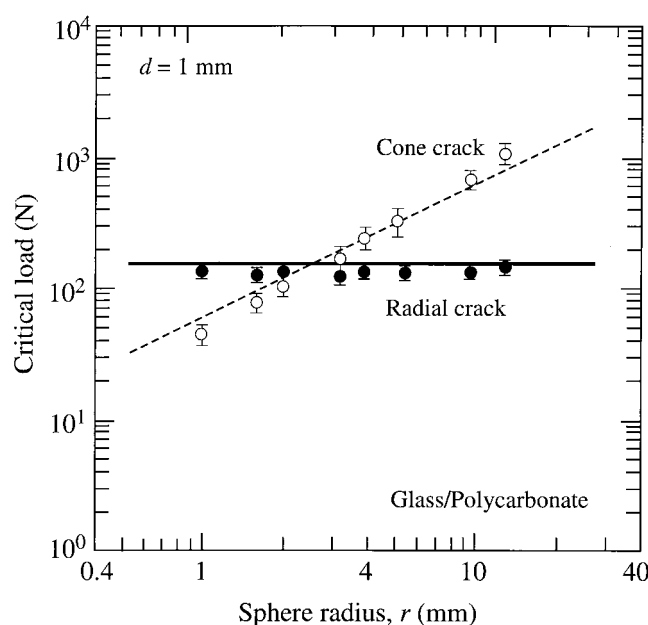


**Fig. 8.** Critical load versus indenter sphere radius  $r$  for soda-lime glass coatings of thickness  $d = 1$  mm on polycarbonate substrates. Filled symbols are  $P_R$  data, unfilled symbols are  $P_C$  data for monoliths (quasiplastic mode not observed). Solid lines are theoretical predictions.

The associated critical loads are strongly dependent on  $d$  ( $P_R \propto d^2$ , Eq. (1)), but are insensitive to  $r$ , reflective of a flexure-dominated field. In thicker coatings ( $d > 0.5$ –2 mm) the material behaves more like a monolith, and either cone cracking or quasiplasticity prevail. The critical loads now depend on  $r$  ( $P_C \propto r$ , Eq. (2);  $P_Y \propto r^2$ , Eq. (3)), but are insensitive to  $d$ . (The different  $r$  dependencies in Eqs. (2) and (3) indicate a brittle–plastic indenter size effect in the near-surface damage.<sup>9</sup>) These dependencies are not exact:<sup>16</sup> the coefficient  $B$  becomes slightly dependent on  $d$ , and  $C$  slightly on the ratio  $a/d$  and hence  $r/d$ ,<sup>20</sup> as the point-loading assumption begins to break down in the region of very thin films (Fig. 1).<sup>20</sup> Coefficients  $A$  and  $D$  in Eqs. (2) and (3) also become slightly dependent on  $d$ , as an increasing flexural component imposes itself on the near-surface contact stress state at intermediate values of  $d$ . Nevertheless, the equations are sufficiently accurate to describe the main trends observed over our data range.

The material parameters that govern the critical loads for the various damage modes are readily identifiable in Eqs. (1)–(3).  $P_R$  for radial cracking in Eq. (1) is controlled primarily by strength  $\sigma_F$ , with comparatively slow dependence on the coating/substrate modulus ratio  $E/E_s$ . (Eq. (1) may be transposed to enable useful estimates of (biaxial) strengths of brittle coatings from  $P_R$  measurements, for any specified  $E/E_s$ .)  $P_C$  for cone cracking in Eq. (2) is controlled by  $T$  and  $E$  (and  $E/E_s$ ). Similarly,  $P_Y$  for quasiplasticity in Eq. (3) is controlled by  $H$  and  $E$  (and  $E/E_s$ ). These are all basic parameters, either obtainable from the literature for most common materials or readily measured by conventional methods.

With the coefficients  $A$ ,  $B$ ,  $C$ , and  $D$  “calibrated” (Section IV), Eqs. (1)–(3) provide simple closed-form relations for *a priori* predictions of the critical loads for first damage in any indenter/coating/substrate system whose basic material parameters are known. (Of course, any practical application of Eqs. (1)–(3) should always be augmented with experimental data on real systems or, at the very least, finite element calculations.) This enables us to construct “design diagrams.” Examples of such diagrams are shown in Figs. 9–11. In these diagrams the solid lines represent the lowest of  $P_R$ ,  $P_C$ , and  $P_Y$  at any  $d$ . To avoid all damage, it is necessary to operate below these bounding solid lines. Figure 9 compares plots for the same glass,  $\text{Al}_2\text{O}_3$  and  $\text{ZrO}_2$  ceramic coating materials examined in the present study (Table I), and for the same polycarbonate base and sphere radius  $r = 3.96$  mm (cf. Figs. (5–7)). The  $\text{ZrO}_2$  has the highest resistance to radial cracking,

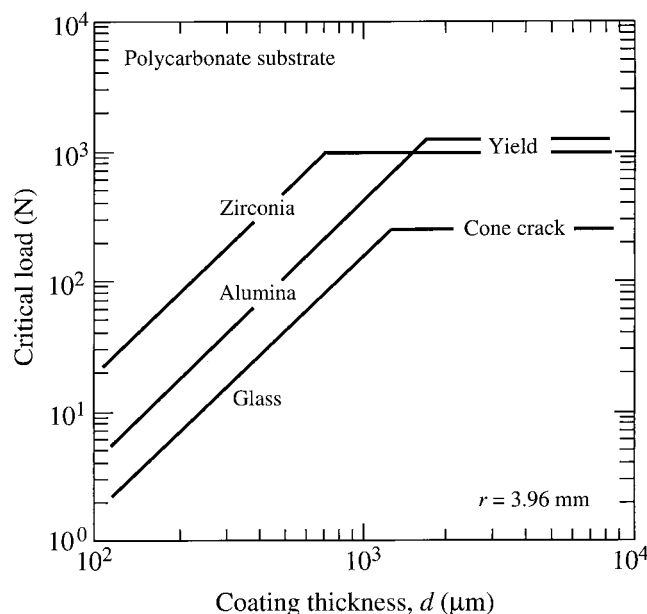


**Fig. 9.** Design diagram. Predicted critical loads, as a function of coating thickness, for the three ceramic/polycarbonate bilayer systems studied. Inclined lines are radial cracking and horizontal lines cone cracking or quasiplasticity, whichever is lower. Plots for  $r = 3.96$  mm.

but its (yield-limited) maximum sustainable load ( $\sim 1000$  N) is no better than that of the  $\text{Al}_2\text{O}_3$ . Figure 10 compares plots for  $\text{Al}_2\text{O}_3$  coatings on substrates of different modulus,<sup>35</sup> again for  $r = 3.96$  mm. Stiffer supports provide higher resistance to fracture initiation, in the thin-coating region where radial cracks dominate. However, this has to be balanced against a reduced capacity for stiffer underlayers to contain cracks once they do initiate.<sup>12,36,37</sup> Finally, Fig. 11 compares plots for three sphere radii  $r$  for  $\text{Al}_2\text{O}_3$  coatings on polycarbonate bases. While the critical loads for radial cracking remain invariant, the maximum sustainable loads are strongly dependent on  $r$ . Clearly, it is important to avoid “sharp” contacts,<sup>38</sup> to ensure that a high resistance to radial fracture is not

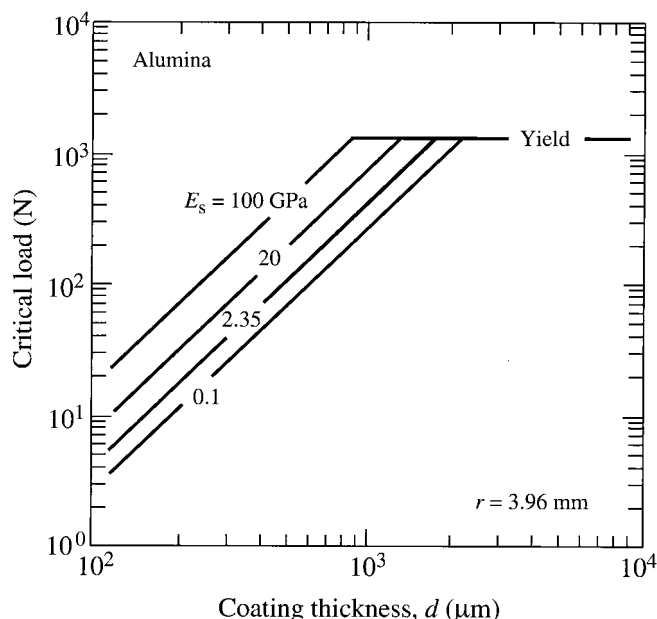


**Fig. 10.** Design diagram. Predicted critical loads, as a function of coating thickness, for  $\text{Al}_2\text{O}_3$  coatings with substrates of different moduli  $E_s$ . Inclined lines are radial cracking and horizontal lines quasiplasticity (cone cracking occurs at higher load). Plots for  $r = 3.96$  mm.

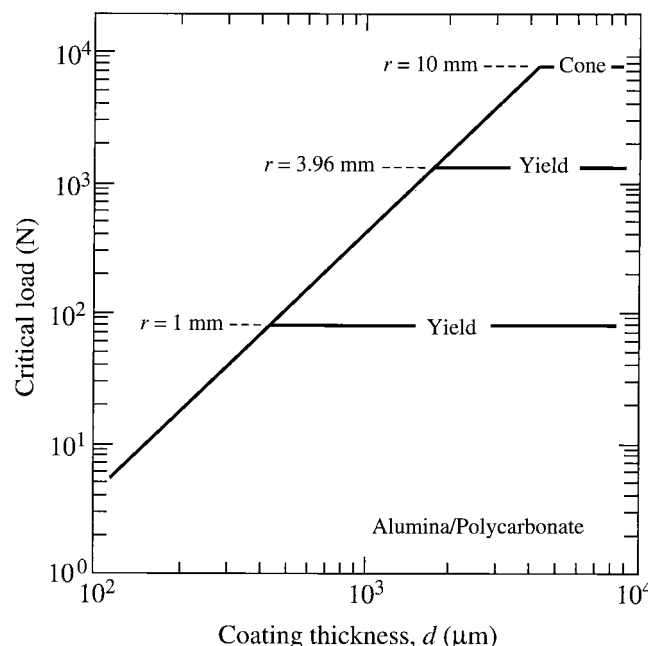


**Fig. 11.** Design diagram. Predicted critical loads, as a function of coating thickness, for  $\text{Al}_2\text{O}_3$ /polycarbonate bilayers subjected to indentation with spheres of different radius. Inclined lines are radial cracking and horizontal lines cone cracking or quasiplasticity, whichever is lower (note transition from yield to cone cracking with increasing  $r$ ).

compromised by premature surface damage in the contact near field.

The appearance of strength  $\sigma_F$  in Eq. (1) raises the issue of the role of surface flaw state, e.g. as-received, polished, abraded, machined, in the critical load  $P_R$  for radial cracking. (As stated in Section II,  $P_C$  and  $P_Y$  are relatively insensitive to flaw state.) Because  $\sigma_F$  varies with the inverse square root of flaw size,  $P_R$  also varies with the inverse square root of flaw size. Thus it is advisable to avoid large surface flaws in the brittle coating, either intrinsic or extrinsic, especially at the lower surface. In this context, the lower surfaces of all-ceramic crowns are deliberately subjected to an abrasive sand-blast treatment during preparation.<sup>4</sup> Our use of abraded surfaces for experimental control means that the  $P_R(d)$  data in Fig. 5 may be regarded as lower-bound estimates of practical load-bearing capacity of glassy coatings, realistically expanding the domain of safe operation to somewhat smaller thicknesses. The effect of flaws on ceramic surfaces needs to be pursued and, where the scatter is large, incorporated into a probabilistic design framework.

### Acknowledgments

The authors wish to thank Herzl Chai, Kee Sung Lee, Antonia Pajares, Pedro Miranda, Fernando Guiberteau and Do Kyung Kim for many discussions and for experimental assistance in many aspects of this work.

### References

- <sup>1</sup>B. R. Lawn, N. P. Padture, H. Cai, and F. Guiberteau, “Making Ceramics ‘Ductile,’” *Science*, **263** 1114–16 (1994).
- <sup>2</sup>B. R. Lawn, “Indentation of Ceramics With Spheres: A Century After Hertz,” *J. Am. Ceram. Soc.*, **81** [8] 1977–94 (1998).
- <sup>3</sup>J. R. Kelly, “Ceramics in Restorative and Prosthetic Dentistry,” *Ann. Rev. Mater. Sci.*, **27** 443–68 (1997).
- <sup>4</sup>I. M. Peterson, A. Pajares, B. R. Lawn, V. P. Thompson, and E. D. Rekow, “Mechanical Characterization of Dental Ceramics Using Hertzian Contacts,” *J. Dent. Res.*, **77** [4] 589–602 (1998).
- <sup>5</sup>J. R. Kelly, “Clinically Relevant Approach to Failure Testing of All-Ceramic Restorations,” *J. Prosthet. Dent.*, **81** [6] 652–61 (1999).
- <sup>6</sup>F. Guiberteau, N. P. Padture, H. Cai, and B. R. Lawn, “Indentation Fatigue: A Simple Cyclic Hertzian Test for Measuring Damage Accumulation in Polycrystalline Ceramics,” *Philos. Mag. A*, **68** [5] 1003–16 (1993).

- <sup>7</sup>F. Guiberteau, N. P. Padture, and B. R. Lawn, "Effect of Grain Size on Hertzian Contact in Alumina," *J. Am. Ceram. Soc.*, **77** [7] 1825–31 (1994).
- <sup>8</sup>H. Cai, M. A. Stevens Kalceff, and B. R. Lawn, "Deformation and Fracture of Mica-Containing Glass-Ceramics In Hertzian Contacts," *J. Mater. Res.*, **9** [3] 762–70 (1994).
- <sup>9</sup>Y.-W. Rhee, H.-W. Kim, Y. Deng, and B. R. Lawn, "Brittle Fracture Versus Quasi Plasticity in Ceramics: A Simple Predictive Index," *J. Am. Ceram. Soc.*, **84** [3] 561–65 (2001).
- <sup>10</sup>S. S. Scherrer and W. G. d. Rijk, "The Fracture Resistance of All-Ceramic Crowns on Supporting Structures With Different Elastic Moduli," *Int. J. Prosthodontics*, **6** [5] 462–67 (1993).
- <sup>11</sup>S. Wuttiphon, B. R. Lawn, and N. P. Padture, "Crack Suppression in Strongly-Bonded Homogeneous/Heterogeneous Laminates: A Study on Glass/Glass-Ceramic Bilayers," *J. Am. Ceram. Soc.*, **79** [3] 634–40 (1996).
- <sup>12</sup>L. An, H. M. Chan, N. P. Padture, and B. R. Lawn, "Damage-Resistant Alumina-Based Layer Composites," *J. Mater. Res.*, **11** [1] 204–10 (1996).
- <sup>13</sup>H. Liu, B. R. Lawn, and S. M. Hsu, "Hertzian Contact Response of Tailored Silicon Nitride Multilayers," *J. Am. Ceram. Soc.*, **79** [4] 1009–14 (1996).
- <sup>14</sup>T. J. Lardner, J. E. Ritter, and G.-Q. Zhu, "Spherical Indentation and Fracture of Glass Plates," *J. Am. Ceram. Soc.*, **80** [7] 1851–62 (1997).
- <sup>15</sup>K. S. Lee, S. Wuttiphon, X. Z. Hu, S. K. Lee, and B. R. Lawn, "Contact-Induced Transverse Fractures in Brittle Layers on Soft Substrates: A Study on Silicon Nitride Bilayers," *J. Am. Ceram. Soc.*, **81** [3] 571–80 (1998).
- <sup>16</sup>H. Chai, B. R. Lawn, and S. Wuttiphon, "Fracture Modes in Brittle Coatings with Large Interlayer Modulus Mismatch," *J. Mater. Res.*, **14** [9] 3805–17 (1999).
- <sup>17</sup>H. Chai and B. R. Lawn, "Role of Adhesive Interlayer in Transverse Fracture of Brittle Layer Structures," *J. Mater. Res.*, **15** [4] 1017–24 (2000).
- <sup>18</sup>Y. G. Jung, S. Wuttiphon, I. M. Peterson, and B. R. Lawn, "Damage Modes in Dental Layer Structures," *J. Dent. Res.*, **78** [4] 887–97 (1999).
- <sup>19</sup>A. Pajares, L. Wei, B. R. Lawn, and C. C. Berndt, "Contact Damage in Plasma-Sprayed Alumina-Based Coatings," *J. Am. Ceram. Soc.*, **79** [7] 1907–14 (1996).
- <sup>20</sup>S. Timoshenko and S. Woinowsky-Krieger, *Theory of Plates and Shells*; Sect. 61. McGraw-Hill, New York, 1959.
- <sup>21</sup>S. S. Scherrer, W. G. D. Rijk, U. C. Belser, and J.-M. Meyer, "Effect of Cement Film Thickness on the Fracture Resistance of a Machinable Glass-Ceramic," *Dent. Mater.*, **10** 172–77 (1994).
- <sup>22</sup>B. R. Lawn, K. S. Lee, H. Chai, A. Pajares, D. K. Kim, S. Wuttiphon, I. M. Peterson, and X. Hu, "Damage-Resistant Brittle Coatings," *Adv. Eng. Mater.*, **2** [11] 745–48 (2000).
- <sup>23</sup>F. C. Frank and B. R. Lawn, "On the Theory of Hertzian Fracture," *Proc. R. Soc. London, A*, **299** [1458] 291–306 (1967).
- <sup>24</sup>B. R. Lawn, *Fracture of Brittle Solids*; Cambridge University Press, Cambridge, U.K., 1993.
- <sup>25</sup>F. B. Langitan and B. R. Lawn, "Hertzian Fracture Experiments on Abraded Glass Surfaces as Definitive Evidence for an Energy Balance Explanation of Auerbach's Law," *J. Appl. Phys.*, **40** [10] 4009–17 (1969).
- <sup>26</sup>S. K. Lee, S. Wuttiphon, and B. R. Lawn, "Role of Microstructure in Hertzian Contact Damage in Silicon Nitride: I. Mechanical Characterization," *J. Am. Ceram. Soc.*, **80** [9] 2367–81 (1997).
- <sup>27</sup>I. M. Peterson, S. Wuttiphon, B. R. Lawn, and K. Chyung, "Role of Microstructure on Contact Damage and Strength Degradation of Micaceous Glass-Ceramics," *Dent. Mater.*, **14**, 80–89 (1998).
- <sup>28</sup>K. L. Johnson, *Contact Mechanics*; Cambridge University Press, London, U.K., 1985.
- <sup>29</sup>B. R. Lawn, D. B. Marshall, P. Chantikul, and G. R. Anstis, "Indentation Fracture: Applications in the Assessment of Strength of Ceramics," *J. Aust. Ceram. Soc.*, **16** [1] 4–9 (1980).
- <sup>30</sup>Y.-G. Jung, I. M. Peterson, D. K. Kim, and B. R. Lawn, "Lifetime-Limiting Strength Degradation from Contact Fatigue in Dental Ceramics," *J. Dent. Res.*, **79** [2] 722–31 (2000).
- <sup>31</sup>A. C. Fischer-Cripps and B. R. Lawn, "Stress Analysis of Contact Deformation in Quasi-Plastic Ceramics," *J. Am. Ceram. Soc.*, **79** [10] 2609–18 (1996).
- <sup>32</sup>P. Miranda, A. Pajares, F. Guiberteau, F. L. Cumbrera and B. R. Lawn, "Contact Fracture of Brittle Bilayer Coatings on Soft Substrates," *J. Mater. Res.*, **16** [1] 115–26 (2001).
- <sup>33</sup>D. K. Kim, Y.-G. Jung, I. M. Peterson, and B. R. Lawn, "Cyclic Fatigue of Intrinsically Brittle Ceramics in Contact With Spheres," *Acta Mater.*, **47** [18] 4711–25 (1999).
- <sup>34</sup>K. S. Lee, Y.-G. Jung, I. M. Peterson, B. R. Lawn, D. K. Kim, and S. K. Lee, "Model for Cyclic Fatigue of Quasi-Plastic Ceramics in Contact with Spheres," *J. Am. Ceram. Soc.*, **83** [9] 2255–62 (2000).
- <sup>35</sup>K. S. Lee, Y.-W. Rhee, D. H. Blackburn, B. R. Lawn, and H. Chai, "Cracking of Brittle Coatings Adhesively Bonded to Substrates of Unlike Modulus," *J. Mater. Res.*, **15** [8] 1653–56 (2000).
- <sup>36</sup>M.-W. He and J. W. Hutchinson, "Crack Deflection at an Interface between Dissimilar Elastic Materials," *Int. J. Solids Struct.*, **25** [9] 1053–67 (1989).
- <sup>37</sup>M. C. Shaw, D. B. Marshall, M. S. Dadkhah, and A. G. Evans, "Cracking and Damage Mechanisms in Ceramic/Metal Multilayers," *Acta Metall. Mater.*, **41** [11] 3311–22 (1993).
- <sup>38</sup>B. R. Lawn and T. R. Wilshaw, "Indentation Fracture: Principles and Applications," *J. Mater. Sci.*, **10** [6] 1049–81 (1975). □